Thermal behaviour of chlorine in nuclear graphite at a microscopic scale

C.E. Vaudey [a,*], N. Toulhoat [a,b,*], N. Moncoffre [a], N. Bérerd [a,c], L. Raimbault [d],
P. Sainsot [e], J.N. Rouzaud [f], A. Perrat-Mabilon [a]

[a] Université de Lyon, Université Lyon 1, CNRS/IN2P3, UMR5822, Institut de Physique Nucléaire de Lyon (IPNL), 4 rue Enrico Fermi, F-69622 Villeurbanne cedex, France
[b] Commissariat à l'Energie Atomique CEA/DEN, Centre de Saclay, F-91191 Gif sur Yvette cedex, France
[c] Université de Lyon, UCBL-IUT A, département chimie, 43 Bd du 11 novembre 1918, F-69622 Villeurbanne cedex, France
[d] Ecole des Mines de Paris, Centre de Géosciences, 35 rue Saint Honoré, F-77305 Fontainebleau cedex, France
[e] Université de Lyon, Université Lyon 1, LaMCoS, INSA-Lyon, CNRS UMR5259, F-69621 Villeurbanne cedex, France
[f] Laboratoire de Géologie de l'Ecole Normale Supérieure, UMR CNRS-ENS 8538, 24 rue Lhomond, F-75231 Paris cedex 5, France

ARTICLE INFO

ABSTRACT

In this paper, we present the study of thermal behaviour of ^{36}Cl in nuclear graphite used in the St. Laurent A2 UNGG reactor (graphite moderated and CO_2 cooled reactor). ^{37}Cl, used to simulate ^{36}Cl displaced from its original structural site by recoil, has been implanted into nuclear graphite samples (energy = 250 keV, fluence = 5×10^{13} at cm^{-2}). The samples have been annealed in the 200–800 °C temperature range and analysed by SIMS. Structural modifications have been controlled by Raman microspectroscopy. This study shows that, in the considered temperature range and for a short annealing duration (4 h), chlorine is released almost athermally. At 500 °C, around 20% of the initial ^{37}Cl content is released. At 800 °C, the release reaches a plateau and the loss of ^{37}Cl is around 30%. Raman microspectroscopy shows that ^{37}Cl implantation induces a structural disorder and that during annealing, the original structure is not completely recovered.

© 2009 Elsevier B.V. All rights reserved.

1. Introduction

The dismantling of the first generation "*Uranium Naturel Graphite Gaz*" French reactors, called UNGG, will produce an important quantity of irradiated graphite waste. According to the French law of June 2006, a specific disposal must be created for this low activity waste. It is therefore necessary to assess the graphite waste long-term behaviour.

Nuclear graphite is manufactured from petroleum coke grains (filler) blended with coal tar pitch acting as a binder. Shaped blocks are formed by extrusion of the blend. They are heat-treated up to about 2800 °C (graphitisation treatment) and polycrystalline graphite is obtained. Blocks, intended for the moderator or reflector, may be further impregnated with pitch, re-baked and regraphitised in order to increase the density. Virgin nuclear graphites have initial densities in the range 1.6–1.8 g cm^{-3}. The difference with graphite crystal (density = 2.265 g cm^{-3}) is due to internal porosity [1]. As a result of mixing of several carbon compounds, this material is structurally heterogeneous at a local scale. Nuclear graphite presents a complex multiscale organisation. It can be locally more or less anisotropic and not completely graphitised. Nuclear graphite has a polycrystalline structure and contains micrometer sized grains. The grains are formed by several more or less oriented crystallites with a size of a few hundreds nanometers. Each crystallite is formed by a triperiodical stacking of graphene planes. Nuclear graphite contains also small amounts of impurities like oxygen, hydrogen, metals and halogens, among them chlorine. Chlorine contents range from some at. ppm to around 50 at. ppm (called pristine chlorine in the following). It could result from graphite purification (elimination of sulphur and metallic impurities) [2], as well as be present as an impurity in coke or pitch.

During reactor operation, the main part of ^{35}Cl is activated into ^{36}Cl [3,4]. Consequently, irradiated nuclear graphite contains ^{36}Cl isotope as an impurity. ^{36}Cl has a long radioactive half-life (about 300,000 years) and is highly soluble in water and mobile in the environment. ^{36}Cl can be released during dismantling and storage. Moreover in the case of long term disposal, it may contribute to a significant dose peak at the outlet after water ingress into the site [5]. The release of ^{36}Cl could have an impact on environment because of the high soil to plant transfer factor of chlorine [6,7]. The release of ^{36}Cl depends on different processes such as water

* Corresponding authors. Present address: IPNL, Bâtiment Dirac, 4 rue Enrico Fermi, 69622 Villeurbanne cedex, France. Tel.: +33 4 72 43 10 63; fax: +33 4 72 44 84 02 (C.E. Vaudey).
E-mail addresses: vaudey@ipnl.in2p3.fr (C.E. Vaudey), nelly.toulhoat@univ-lyon1.fr (N. Toulhoat).

saturation or water access into graphite pore spaces. Moreover, the solubilisation of ^{36}Cl is controlled by its chemical form, as well as its properties regarding diffusion and retention. In order to be able to identify and quantify the release mechanisms of ^{36}Cl into water, it is necessary to determine its location and speciation before any contact between graphite and water i.e. before dismantling and disposal. Two main factors may determine chlorine's behaviour: temperature and graphite oxidation (thermal or radiolytic) [8].

In this paper, we present results concerning the thermal behaviour of chlorine in virgin nuclear graphite using a micrometric approach. This study is based on the use of ion implantation. This technique has been widely used to study the lattice location, the diffusion and the release of fission and activation products in nuclear materials [9–12]. In this study, ^{37}Cl is implanted to simulate the behaviour of ^{36}Cl displaced from its original site through recoil during reactor operation. Indeed, ^{36}Cl is mainly produced by neutron capture according to the $^{35}Cl(n, \gamma)^{36}Cl$ reaction having a strong cross section for thermal neutrons (around 33 barns) and providing a series of γ-rays spanning a wide energy range from 517 to 8579 keV [13]. The recoil energy of ^{36}Cl is calculated according to Coltman et al. [14]:

$$E_r = 5.4 \times 10^{-4} \quad E_\gamma^2/A \tag{1}$$

with E_r, the recoil energy in MeV, E_γ, the gamma energy in MeV and A, the atomic mass. It leads to a chlorine recoil energy value ranging from 4 eV for a 0.5 MeV gamma-ray to 1.1 keV for a 8.6 MeV gamma-ray. This recoil energy is most of the time, large enough to displace the ^{36}Cl atom from its equilibrium position, since a mean energy of 25 eV is sufficient to displace an atom from its lattice site [15]. The displaced ^{36}Cl will be a free uncharged atom or an electrically charged species. In either of these forms, ^{36}Cl will be extremely chemically reactive and will form bounds with the first other species it encounters [16]. In nuclear graphite, chlorine will be able to react with carbon (major constituent), oxygen (around 1%) and metals (some ppm at.). Similarly, the implanted ^{37}Cl is likely to create bounds with the nuclear graphite matrix elements. The distribution of ^{37}Cl has been followed by Secondary Ion Mass Spectrometry (SIMS). The evolution of the graphite structure after ^{37}Cl implantation, and after the thermal treatments has been followed by Raman microspectroscopy.

2. Experimental

2.1. Samples

Several samples of virgin nuclear graphite (pile grade) used in the French nuclear reactor Saint Laurent A2 (graphite moderated and CO_2 cooled reactor) have been studied (Fig. 1). Two kinds of samples have been investigated. Both have been cut in a same block (Fig. 2a). The first one, called XY, contains grains preferentially oriented perpendicularly to the spinning axis. The second one, called Z, contains grains preferentially oriented along the spinning axis. As a consequence, the XY plane contains more inter crystallite pores than the Z plane (Fig. 2b). The sample surfaces (around 1 cm^2) have been polished to the micrometer.

2.2. Sample implantations and annealings

After manual polishing, the samples have been annealed at 1000 °C during 8 h under secondary vacuum in order to anneal defects induced by polishing.

In order to study the migration properties of chlorine at a microscopic scale, ^{37}Cl has been implanted into the polished sample surfaces. $^{37}Cl^+$ ions have been implanted into the polished surfaces using the 400 kV ion implanter of the Institute of Nuclear Physics of Lyon (IPNL, France). Target samples were cooled to 15 °C during implantation. The implantations have been performed at a fluence of 5×10^{13} at. cm^{-2} and at an energy of 250 keV. The ^{37}Cl projected range (R_p) has been calculated using the Stopping and Range of Ions in Matter (SRIM), based on Monte Carlo calculations, software [17]. The SIMS analyses have been performed at the scale of nanoporous graphite grains. A matrix density of 2.2 g cm^{-3} has been chosen for the calculations because we assume that this density is representative of the nanoporous grains density. The implantation results in a nearly Gaussian profile with a projected range R_p centred around 200 nm and a maximum atomic concentration around 50 ppm. The implantation fluence was chosen to limit the creation of defects and the effects due to release and/or trapping usually observed at higher fluences for volatile elements. Indeed, the value of displaced atoms at the maximum of the defect profile in the implanted volume, calculated with SRIM, is around
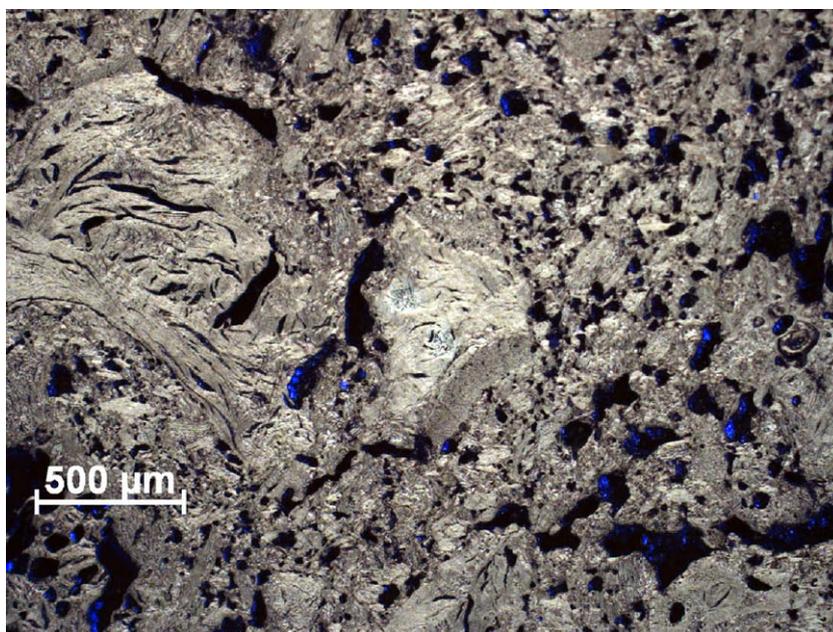

Fig. 1. Picture of the surface of St. Laurent A2 nuclear graphite obtained by optical microscope.
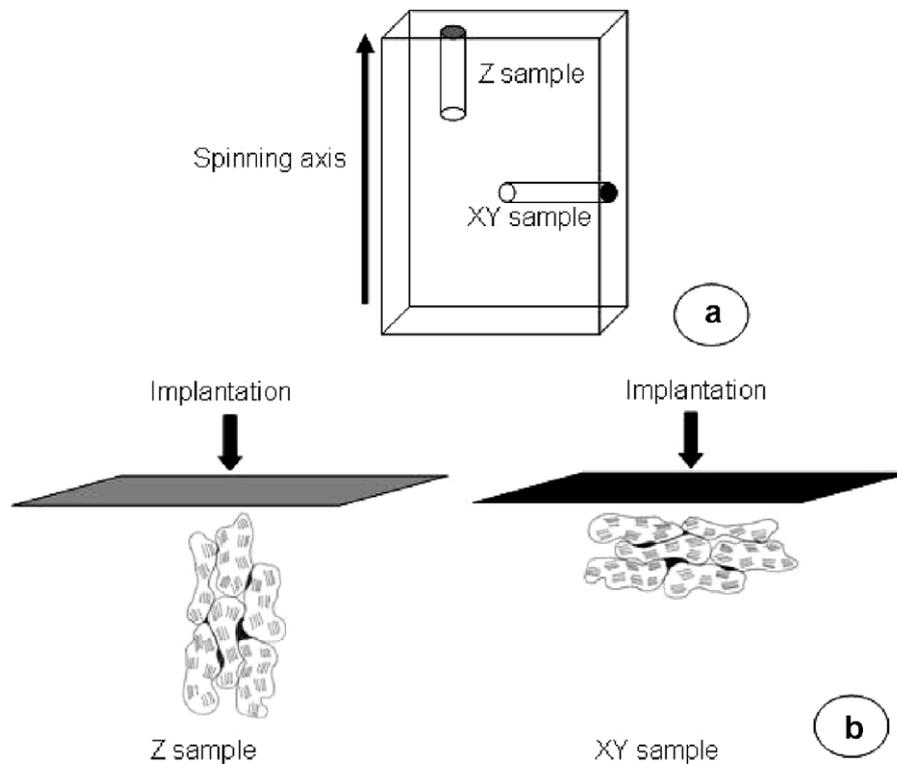
Fig. 2. (a) Sketch of XY and Z samples in a block of St. Laurent A2 nuclear graphite (b) Sketch of ^{37}Cl implantation into XY and Z samples.

0.02 dpa (displacement per atom). It is however high enough to get a significant signal of the implanted versus the pristine chlorine during SIMS depth profiling.

In order to study the effect of graphite texture on the release of chlorine, two implantation directions have been considered for the implantations. The first implantation has been performed in the plane Z (along the spinning axis) and the second one in the plane XY (perpendicularly to the spinning axis) (Fig. 2b).

After implantation, the samples have been annealed at temperatures ranging from 200 °C to 1000 °C during 4 h under argon flux. For each annealing, the furnace was pre-set to the requested temperature before entering the samples.

2.3. Analysis

SIMS experiments were carried out using the CAMECA IMS 6f SIMS facility at the "Ecole des Mines de Paris" in Fontainebleau (ENSM-P, France) to analyse ^{37}Cl depth profiles on the implanted and annealed samples. The focused primary beam was rastered over an area of $150 \times 150 \ \mu m^2$ on the sample surface. Secondary ions were collected from a smaller region (8 μm in diameter) located at the center of the sputtered area to minimize crater-edge effects. Accelerating voltages were set to 10 kV in the primary ion source and to −4.5 kV on the sample holder, resulting in rastering of a 14.5 keV primary cesium ion beam of about 8 nA intensity. Negative secondary ions detected as ^{37}Cl$^-$ (mostly implanted ions), ^{35}Cl$^-$ (initial impurities) and ^{12}C$^-$ (matrix ions) were collected. The mass resolution $M/\Delta M$, where M is the molecular mass of an isotope, was set to 800 to avoid a major polyatomic interference due to C$_3$H. As the ^{12}C$^-$ signal does not vary with the annealing time, we used it as an internal reference to normalise the ^{37}Cl$^-$ signal. Pre-implantation ^{37}Cl contribution (initial impurities) has been computed from ^{35}Cl$^-$ signal and subtracted from total ^{37}Cl$^-$ signal to obtain the actual ^{37}Cl implanted concentration. ^{37}Cl intensities have been obtained as a function of sputtering time. For each sput-

tered profile, the depth scale has been determined by measuring the crater depth by optical interferometry at the "Institut National des Sciences Appliquées" (INSA Lyon, France), with Microsurf 3D interferometer of Fogale nanotech. The depth resolution was estimated to be around 50 nm at the bottom of the craters. This value is mainly due to the residual sample surface roughness (0.2 μm) and to differential erosion rates due to local heterogeneities (more or less graphitised zones in relation with the different carbon compounds). ^{37}Cl intensities have been converted to ^{37}Cl atomic concentrations, by normalising the areas of the as implanted SIMS profiles by the areas of the profiles calculated with SRIM.

Finally, the evolution of graphite structure has been controlled, at each step of the treatments (implantation and post-thermal treatments), by Raman microspectroscopy, at the "Ecole Normale Supérieure de Paris" (ENS, France), with a Renishaw InVia spectrometer using a laser wavelength of 514.5 nm. The analysed surface and mean depth were respectively around 1 μm^2 and 0.2 μm.

3. Results and discussion

3.1. Temperature dependent evolution of chlorine concentration

Fig. 3 displays the comparison between the SRIM calculated profile and the as implanted experimental ^{37}Cl profiles obtained by SIMS for both samples. Table 1 presents the characteristics of the concentration profiles (Full Width at Half Maximum (FWHM), mean value R_p and integrated surface S) for the as implanted and annealed samples. The comparison of the experimental profiles and the SRIM profile shows (Fig. 3): (1) A shift of the Z experimental profile peak maximum with respect to the SRIM profile; the shift is lower or of the same order as the depth resolution; (2) A spreading of both experimental profiles Z and XY over depth compared to the SRIM profile. The FWHM of the SRIM, as implanted Z and XY profiles are respectively of 84, 95 and 110 nm; we assume that this spreading results from the porous texture of graphite.
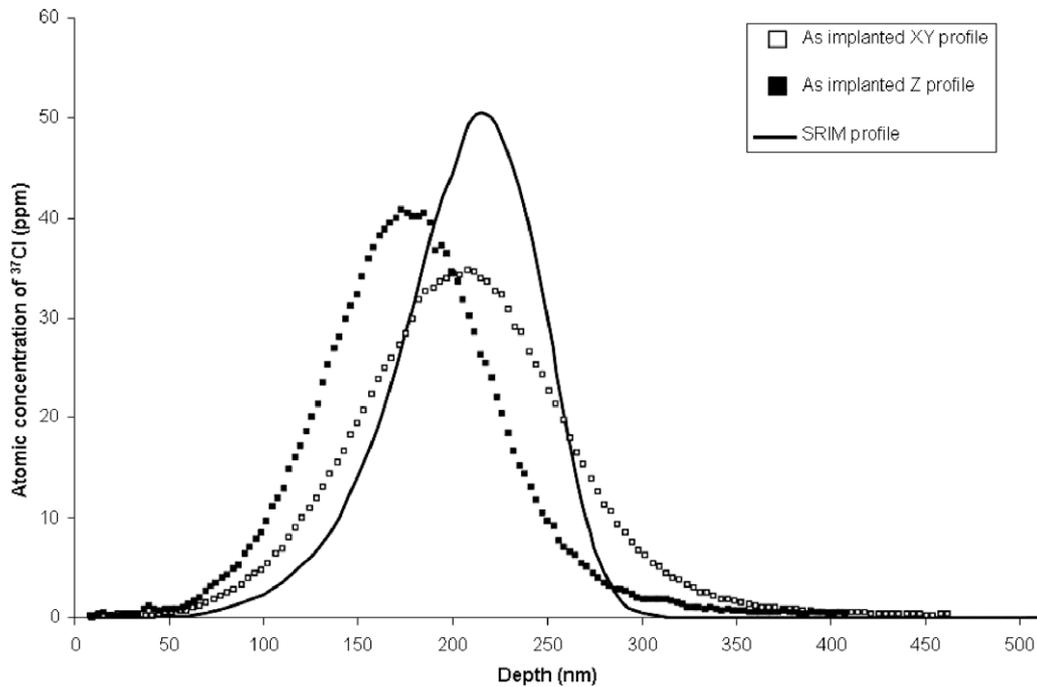
Fig. 3. ^{37}Cl calculated profile simulated by SRIM software and ^{37}Cl implanted experimental profiles measured by SIMS for XY and Z samples of St. Laurent A2 nuclear graphite.

Table 1
Full Width at Half Maximum FWHM, projected range R_p and integrated surface S for as implanted and annealed samples of XY and Z St Laurent A2 nuclear graphite.

	Annealing temperature (°C)	FWHM (nm)	R_p (nm)	S (ppm nm)
Z	As implanted	95	175 ± 20	1530
	200	95	195 ± 20	1310
	400	105	185 ± 20	1390
	600	100	170 ± 15	1220
XY	As implanted	110	190 ± 15	1180
	600	110	175 ± 20	960
	800	100	175 ± 20	996
	1000	105	210 ± 15	866

Moreover, the larger spreading of the XY profile compared to the Z one is probably due to the fact that the XY plane contains more pores forming preferential paths for chlorine implantation.

The depth profiles of ^{37}Cl have been measured as a function of annealing temperature from 200 °C to 1000 °C. Fig. 4a and b display the as implanted ^{37}Cl profile and the profiles after annealing for both samples. In any case, no significant spreading of the distributions, nor shift of the R_p is observed (as confirmed in Table 1). Only a decrease of the integrated peak surface is observed as a function of annealing temperature. Consequently, the main migration process is chlorine release. Table 2 displays, for each annealing temperature and each sample, the ratio C_T/C_0, the ^{37}Cl release percentage and k the release kinetic constant (in s^{-1}) calculated according to the following formula:

$$C_T/C_0 = \exp(-k\Delta t) \qquad (2)$$

with C_T, the quantity of ^{37}Cl in ppm after annealing at a temperature T in K, C_0, the as implanted quantity of ^{37}Cl, Δt, the annealing duration in s. This table shows that chlorine is already notably released at a low temperature around 200 °C. For the XY sample, the release increases with temperature up to 800 °C where it reaches a plateau with a maximum loss around 30%. This plateau is observed even for longer annealing times of 8 or 12 h (not shown here). Moreover, the rele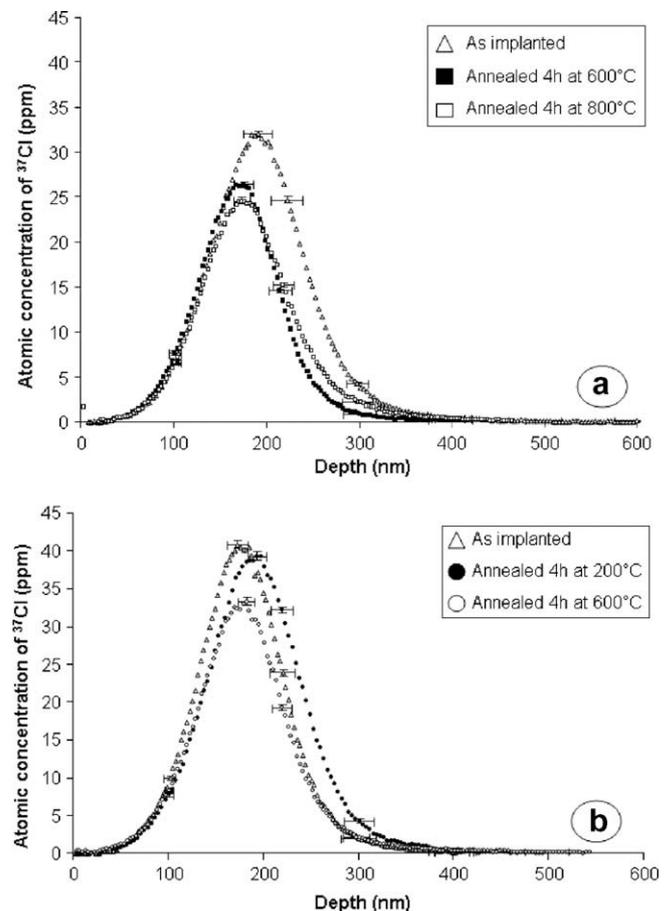ase of chlorine is generally more important in sample XY compared to sample Z (Fig. 5). This could indicate that the inter crystallite pores are also preferential paths for chlorine release.

Fig. 4. SIMS profiles of as implanted ^{37}Cl and after annealing for (a) XY and (b) Z samples of St. Laurent A2 nuclear graphite.

Table 2
CT/C0 ratio, [37]Cl release percentages and k release kinetic constant for XY and Z samples of St. Laurent A2 nuclear graphite at different annealing temperatures for an annealing time of 4 h. The associated errors correspond to statistical uncertainties.

Annealing temperature (°C)	Sample	C_T/C_0	[37]Cl release (%)	Release constant k (s^{-1})
200	XY	0.81 ± 0.19	19	$(1.5 \pm 1.9) \times 10^{-5}$
	Z	0.84 ± 0.05	15	$(1.2 \pm 0.4) \times 10^{-5}$
400	XY	0.64 ± 0.17	35	$(3.0 \pm 1.7) \times 10^{-5}$
	Z	0.88 ± 0.03	12	$(8.7 \pm 1.9) \times 10^{-6}$
600	XY	0.70 ± 0.03	29	$(2.4 \pm 0.2) \times 10^{-5}$
	Z	0.81 ± 0.04	19	$(1.5 \pm 0.3) \times 10^{-5}$
800	XY	0.71 ± 0.02	29	$(2.4 \pm 0.1) \times 10^{-5}$
	Z	0.81 ± 0.13	19	$(1.5 \pm 1.2) \times 10^{-5}$
1000	XY	0.71 ± 0.17	29	$(2.4 \pm 1.2) \times 10^{-5}$
	Z	0.70 ± 0.11	30	$(2.5 \pm 1.5) \times 10^{-5}$

The results have been plotted in an Arrhenius plot displaying the release constant k versus the inverse of annealing temperature for both samples (Fig. 6). This plot shows that the release follows a general trend and a mean activation energy could be calculated. The activation energy E_a has been calculated using the Arrhenius law:

$$k = k_0 \exp(-E_a/k_B T) \tag{3}$$

with k_0, the initial release kinetic constant in s^{-1}, E_a, the activation energy of [37]Cl release in eV, $k_B = 8.65 \times 10^{-5}$ eV K^{-1} the Boltzmann constant, T, the annealing temperature in K. The resulting activation energies E_a, according to Eq. (3), are equal to 0.01 ± 0.01 eV for the XY sample and to 0.04 ± 0.02 eV for the Z sample. These values show that, in the considered temperature range and for annealing times of 4 h, the release of chlorine is athermal.

3.2. Structural evolution of graphite during annealing: Raman microspectroscopy

The structural evolution of graphite has been followed using Raman microspectroscopy. Fig. 7a and b represent the virgin graphite, the implanted graphite and the evolution of Raman spectra for sample XY as a function of annealing temperature. The comparison of the spectra shows that: (1) The virgin graphite (Fig. 7a) displays
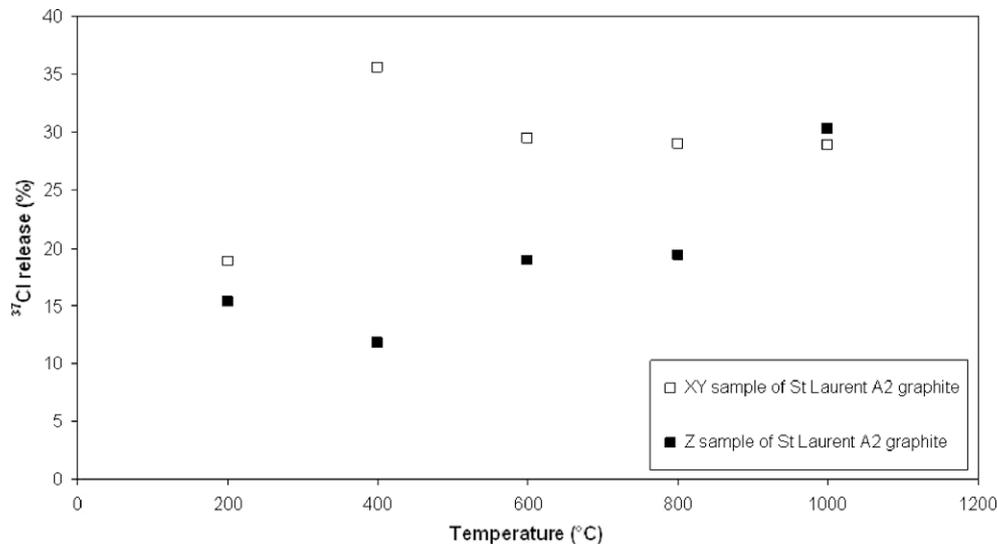

Fig. 5. [37]Cl release for both planes of St. Laurent A2 nuclear graphite.

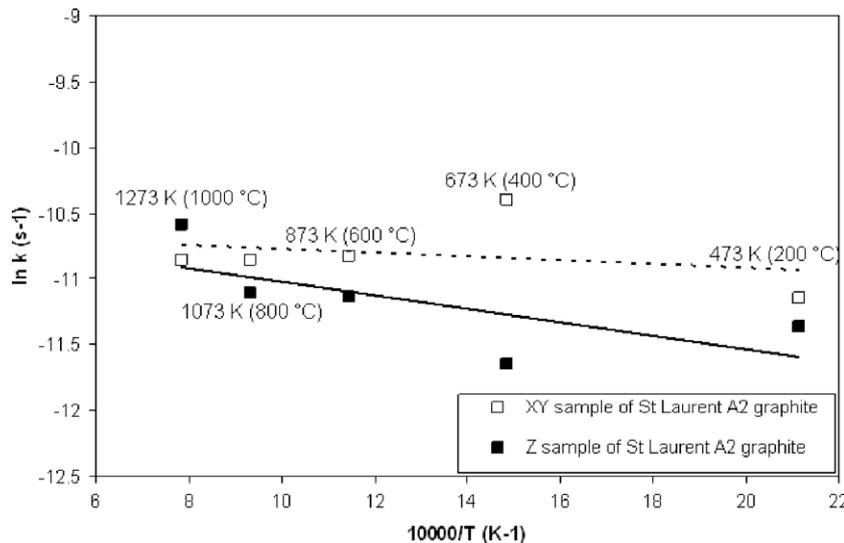**Fig. 6.** [37]Cl release as a function of inverse annealing temperature for an annealing time of 4 h for St. Laurent A2 nuclear graphite XY and Z.
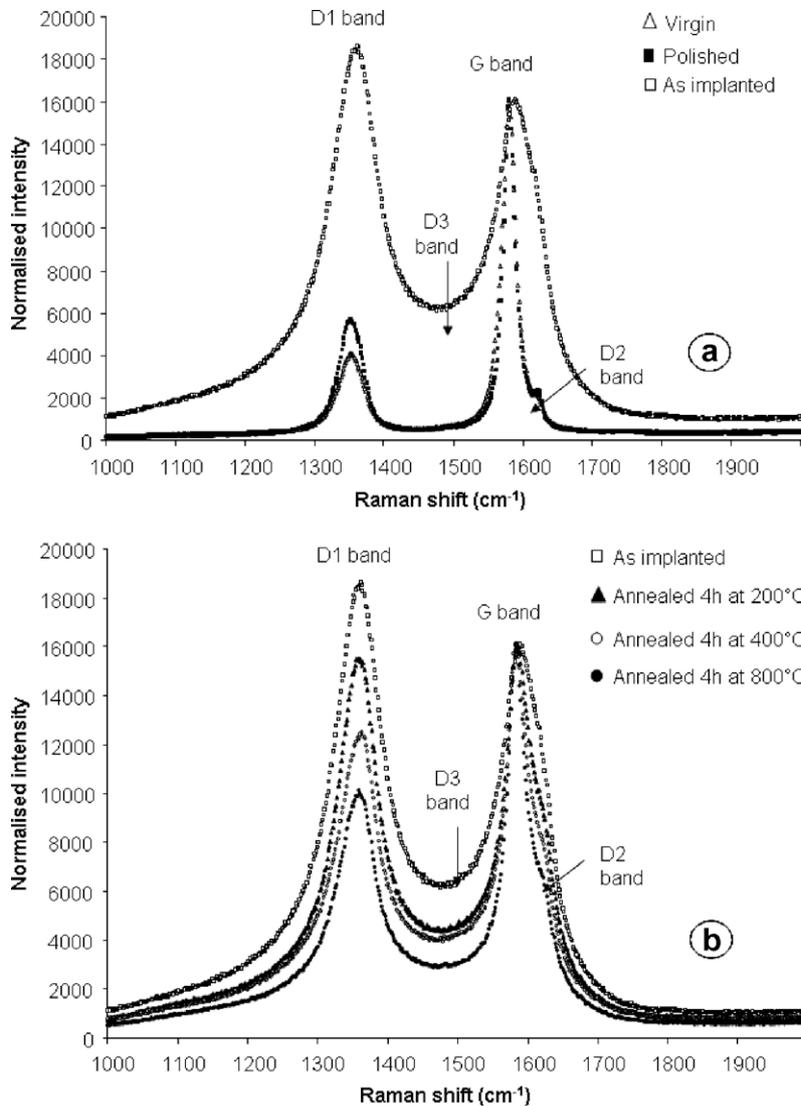
Fig. 7. Raman spectra of St. Laurent A2 nuclear graphite XY (a) virgin, (a) polished, (a and b) implanted and (b) annealed samples.

3 main bands: the G band centred at around $1580\ cm^{-1}$ corresponding to the "graphite" band (E_{2g} mode) and two bands, called D1 and D2, centred respectively at around 1350 and $1620\ cm^{-1}$ corresponding to defect bands [18–20]; (2) polishing (Fig. 7a) increases the D1 and D2 bands as a consequence of the decrease of crystallite sizes as well as a probable modification of the interlayer spacing distribution [21]; (3) implantation (Fig. 7a and b) results in a strong increase of D1 and D2 bands and induces a new D3 defect band located around $1500\ cm^{-1}$. Such an increase of the D/G surface ratio probably corresponds to a crystallite size decrease [18,22]. In fact, during the implantation, covalent bonds of sp^2 carbons of aromatic rings are broken and covalent bonds (in-plane or between different graphene layers) are created. The size of the coherent domains decreases [23]. The same kind of defects has been observed by Tanabe et al. [24] during graphite irradiation. Irradiation with neutrons or ions results in discrete vacancies and interstitials situated in and between the basal planes and are also likely to include sp^3 carbons. At high fluences or with heavy ion irradiation, the in-plane defects accumulate, resulting in bending of basal planes and three dimensional defect clusters. (4) During annealing (Fig. 7b), the intensities of the defect bands decrease but, even at 800 °C and after 4 h annealing, the original structure is not completely recovered. This progressive and incomplete restructuration of nuclear graphite could be correlated to the release of 30% of the implanted ^{37}Cl. This observation is in agreement with the results obtained by Elman et al. who observe a restructuration of Highly Oriented Pyrolytic Graphite after annealing of implanted samples [23].

4. Conclusion

This paper aimed to study the thermal behaviour of ^{36}Cl in the Saint Laurent A2 nuclear graphite at a micrometric level. Following main results have been obtained:

(1) SIMS experiments show that the thermal release of ^{37}Cl, used to simulate ^{36}Cl displaced from its original structural site by recoil, takes place already at 200 °C. For an annealing time of 4 h and at 500 °C (temperature corresponding to mean operating conditions), around 20% of the implanted chlorine is released. The very low activation energy (<0.1 eV) shows that chlorine loss is athermal. The release reaches a plateau around 30% at 800 °C. Open pores likely form preferential paths for chlorine release.

(2) Raman microspectroscopy experiments show that the introduction of ^{37}Cl induces the creation of defects. The progressive release of ^{37}Cl during annealing is correlated to the partial recovery of the initial structure.

Our results are in agreement with those of Clayton et al. [16] obtained on irradiated graphites. These authors measured a rapid release around 50% of the initial chlorine in Magnox and 30% in AGR reactors. Moreover, they suggest that the further 40% of the remaining chlorine is released over the reactor lifetime. All these results are in favour of the existence of two chlorine chemical forms of different thermal stabilities. It is likely that during reactor operation the more labile fraction is rapidly released. Complementary experiments are underway in order to confirm this hypothesis and to take into account the corrosion effects.

Acknowledgements

References

[1] C.W.E. Addison, S. Barlow, M.A. Bassett, J. Buffery, R. Burcl, A.G. Davies, M. Dubourg, V. Fomin, J.L. Gonzalez Gomez, G. Holt, J.J. Kelly, B.J. Marsden, P.C. Minshall, A. Morales, E. Motokumi, E. Mulyanto, G.B. Neighbour, F. Pineau, P. Poskas, A. Romenkov, M. Shirakawa, A. Suvorov, Yu.A. Verzilov, A.J. Wickham, S.J. Wisbey, M. Wise, Characterisation, Treatment and Conditioning of Radioactive Graphite from Decommissioning of Nuclear Reactors, first ed., IAEA TEC DOC 1521, Austria, September 2006.
[2] P. Cornuault, Génie nucléaire, modérateurs, graphite, Société des Electrodes Réfractaires Savoie, first ed., 1981.
[3] F.J. Brown, J.D. Palmer, P. Wood, Nuclear graphite waste management, in: Proceedings of Manchester IAEA Technical Committee meeting, United Kingdom, first ed., October 1999.
[4] C. Colle, C. Adam, Fiche Radionucléide IRSN, 2002.
[5] P. Toulhoat, Scientific Bases for Nuclear Waste Management XXX Mat. Res. Soc. Symp. Proc. 985 (2007) 0985-NN07-02.
[6] S.C. Sheppard, L.H. Johnson, B.W. Goodwin, J.C. Tait, D.M. Wuschke, C.C. Davison, Waste Manage. 16 (1996) 607.
[7] B.D. Amiro, S.C. Sheppard, F.L. Johnston, W.G. Evenden, D.R. Harris, Sci. Total Environ. 187 (1996) 93.
[8] J. Wright, Gas chemistry in nuclear reactors and large industrial plant, in: A. Dyer (Ed.), Proceedings of Salford, first ed., London, April 1980.
[9] H.j. Matzke, H. Blank, M. Coquerelle, K. Lassmann, I.L.F. Ray, C. Ronchi, C.T. Walker, J. Nucl. Mater. 166 (1989) 165.
[10] H.j. Matzke, A. Turos, J. Nucl. Mater. 188 (1992) 285.
[11] L. Thomé, J. Jagielski, C. Binet, F. Garrido, Nucl. Instrum. Methods Phys. Res. B 166–167 (2000) 258.
[12] Y. Pipon, N. Toulhoat, N. Moncoffre, H. Jaffrézic, S. Gavarini, P. Martin, L. Raimbault, A.M. Scheidegger, Radiochim. Acta 94 (2006) 705.
[13] G.L. Molnar, Z.S. Revay, T. Belgya, Nucl. Instrum. Methods Phys. Res. B 213 (2004) 32.
[14] R.R. Coltman Jr., C.E. Klabunde, D.L. McDonald, J.K. Redman, J. Appl. Phys. 33 (1962) 3509.
[15] S. Blow, J. Phys. D: Appl. Phys. 4 (1971) 1107.
[16] A.M. Clayton, A. Harper, C.J. Wheatley, AEA Technology, Behaviour of chlorine in nuclear graphites, UK NIREX report T/REP/20121/P/04, fourth ed., 1996.
[17] J.F. Ziegler, J.P. Biersaack, U. Littmark, The Stopping and Range of Ions in Solids, first ed., Pergamon Press, New York, 1985.
[18] F. Tuinstra, J. Koeing, J. Chem. Phys. 53 (1970) 1126.
[19] J.N. Rouzaud, A. Oberlin, Thin Solid Films 105 (1983) 75.
[20] A. Sadezky, H. Muckenhuber, H. Grothe, R. Niessner, U. Pöschl, Carbon 43 (2005) 1731.
[21] M. Nakamizo, K. Tamai, Carbon 22 (1984) 197.
[22] C. Bény, J.N. Rouzaud, Characterisation of carbonaceous materials by correlated electron and optical microscopy and Raman microspectroscopy, Scanning Electron Microscopy, first ed., SEM Inc., Chicago, 1985.
[23] B.S. Elman, H. Mazurek, M.S. Dresselhaus, G. Dresslhaus, Mater. Res. Soc. 7 (1982) 425.
[24] T. Tanabe, T. Maruyama, M. Iseki, K. Niwase, H. Atsumi, Fusion Eng. Des. 29 (1995) 428.